Magazine of Civil Engineering

ISSN 2712-8172

journal homepage: http://engstroy.spbstu.ru/

DOI: 10.34910/MCE.102.4

Performance of two-way hinges in reinforced concrete structures

S. Chahal*[a]*, O. Baalbaki[b], Y. Temsah[b], H. Ghanem[b], Z. Abu Saleh[c]

[a] *Order of Engineers and Architects, Tripoli, Lebanon*

[b] *Beirut Arab University, Beirut, Lebanon*

[c] *Rafic Hariri University, Beirut, Lebanon*

[*] *E-mail: safwanchahal79@gmail.com*

Keywords: two-way hinge, reinforced concrete, finite element method, load-displacement curve, amplification factor, shear friction

Abstract. Two-way hinges are frequently practiced in bridge columns aiming to avoid the transfer of bending moment to the foundation. The reduction of the concrete column section over a very small height portion is mainly sufficient to create a hinge like behavior. Currently, ACI Code proposes an amplification factor, limited to two, to account for the increasing of the hinge axial capacity due to the column confinement effect. The shear capacity of two-way hinges is defined as well by the shear friction theory imposed by the code. This paper presents a finite element analysis of two-way hinges to evaluate their behaviors. The experimental data were taken from a recent experimental investigation of two way hinges specimens subjected to axial load only. A numerical analysis was done using ABAQUS software. Based on the good convergence between the numerical and experimental results, a further analysis was conducted to investigate the hinge behavior under the simultaneous effect of axial and lateral loads. It was observed that the tri-axial stresses and confinement provided by the larger area strengthen the throat region, and the axial capacity of the hinge is amplified by a confinement factor equal to three. Furthermore, the confining stress produced by the column on the throat increased the hinge shear capacity more than what the code indicates.

1. Introduction

Concrete hinges have been perfectly used in civil engineering structures for nearly 120 years. They are used to either reduce bending moment transferred to the foundations or redistribute the forces and stresses applied. A recent literature in bridge construction mentioned that Freyssinet and Mesnager concrete hinges are the most developed hinges in the different types of bridge applications since the early last century [1].

Hinges are produced by different means. The reduction of the concrete column cross section over a very small height portion is enough to create a hinge like behavior. The dowel bars are extended from the footing into the column [2]. The stress induced by the bending moment in the smaller section leads the structure to attain the maximum capacity quickly. Consequently, the cracks appear and the section is not capable of sustaining further moment [3].

Two types of hinges are commonly used in bridge construction: one-way and two-way hinges. One-way hinge transmits moment in the strong direction, whereas the moment transferred in the other direction is practically neglected [4–6]. However, two-way hinge restricts the moment transfer in both directions, and thereby reduce the size and cost of the foundation [7–9]. Whereas, previous studies concluded that although the moment at the hinge was not totally neglected, it was substantially lower than the moment capacity of the full section. Thereby, the hinge moment is required to account for in design [2].

Another advantage of using a two-way hinge is the low cost of repairing a damaged two-way hinge compared to that of a damaged full moment connection [10].

Recent researches emphasized that hinges performed a moment-free connections while transferring shear and axial loads, and exhibited large rotations without afflicting their performance [11–12]. Likewise, pipe pins hinge showed well performance in transferring the shear forces to the footing through the pipes interaction and friction [4–5, 13–14]. The well confinement of the two-way hinge by the upper column and the lateral

Chahal, S., Baalbaki, O., Temsah, Y., Ghanem, H., Abu Saleh, Z. Performance of two-way hinges in reinforced concrete structures. Magazine of Civil Engineering. 2021. 102(2). Article No. 10204. DOI: 10.34910/MCE.102.4

reinforcement allows the throat region to maintain large strains [15–16]. Besides, a past study demonstrated that the compressive strength of one-way hinge was largely increased by the confinement provided by the upper column and the lower footing surfaces [2].

However, the effect of tri-axial confinement on the two-way hinge capacity is not extensively discussed in current codes and literature. Therefore, this paper comes to present a numerical investigation of two-way hinges in reinforced concrete members. The experimental data were taken from a recent experimental investigation of two-way hinges specimens subjected to axial load only [17]. A numerical analysis was done using ABAQUS software. Following the good convergence between the numerical and experimental results, a further analysis was conducted to investigate the hinge behavior under the combined effect of axial and lateral loads.

The objectives of this research is to investigate the behavior and the failure modes of two-way hinges subjected simultaneously to axial and lateral loads, as well as to understand the confinement effect imposed by the larger concrete column area on the smaller hinge region, and ultimately to introduce a codified guideline design method of two-way hinges in reinforced concrete structures.

2. Method

2.1. Introduction

The input data used in the numerical analysis are the experimental results performed by Chahal et al. (2019), at Beirut Arab University, Lebanon [17]. The experimental program was composed of eighteen 1/3-scale specimens of two-way reinforced concrete hinges divided into three major series, each consisted of six specimens as provided in Table 1. A 300 mm × 300 mm square footing was used in all cases, with 300 mm height, reinforced by a mesh of 4ϕ14 in the both directions. A 70 mm × 70 mm square hinge area (A_h), with 30 mm thick, and reinforced by 4ϕ10 is used in all models as well. The area of the column (A_c) was accordingly changed to evaluate to effect of different confinement levels. Thus, the ratio $\sqrt{A_c / A_h}$ ranged between 2 and 4 throughout the case. The sizes of specimens are detailed in Fig. 1. The specimens are subjected to an increasing axial load only.

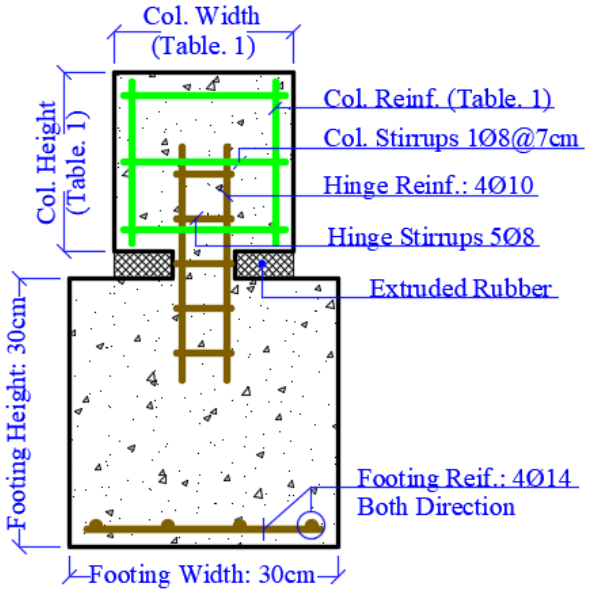

Figure 1. Specimen detail.

Table 1. Characteristics of specimens.

Specimen			Square Column		
Concrete Compressive Strength, f'c (MPa)					$\sqrt{A_c / A_h}$
22	32	40	Width ; Height (mm)	Reinforcement (mm²)	
CS14-22	CS14-32	CS14-40	140	4ϕ12	2.00
CS20-22	CS20-32	CS20-40	200	4ϕ14	2.86
CS21-22	CS21-32	CS21-40	210	8ϕ12	3.00
CS23-22	CS23-32	CS23-40	230	8ϕ12	3.29
CS25-22	CS25-32	CS25-40	250	8ϕ12	3.57
CS28-22	CS28-32	CS28-40	280	8ϕ14	4.00

2.2. Modeling methodology

As indicated earlier, the advanced finite element software ABAQUS was used in the analysis. The standard linear volumetric element type C3D8R with a hexahedral shape was used to model the concrete members as illustrated in Fig. 2. This is an 8 nodded element type with a reduced integral and hourglass control, which is the optimal mesh type to simulate the concrete members and to give the most accurate results with the least run time [18–19]. Steel was assigned as plastic material with a strain hardening curve. As shown in Fig. 3, the standard linear wire truss element type T3D2 was used to model the reinforcement and to prevent any unwanted bending moments. This element type takes axial forces only.

A rigid body constrain between the top of the column and a reference point was assigned. This is to avoid any stress concentration or singularities upon loading. A displacement controlled analysis was proposed to determine the behavior of the cases considered. The models were analyzed using Static/Risk analysis in ABAQUS. A uniformly increasing imposed axial displacement of 20 mm was applied. This is much greater than the failure displacement of all cases. The corresponding reactions were then recorded and plotted.

The bottom of the footing was assigned a fixed boundary condition. It was restrained against translation in all directions. This is to forbid the formation of bending moment which may causes tilting of the footing. Hinged columns usually are stable in structures as they are braced by each other. To avoid such instabilities, and to prevent the formation of bending moments on the column, the top of the column was assigned a restrain against lateral movement.

An embedment constrain was assigned to the steel reinforced in the concrete. This constrain ensures full bond and strain compatibility between the concrete and steel. No direct steel slippage properties were assigned to the reinforcement or to the interface between the concrete and steel reinforcement.

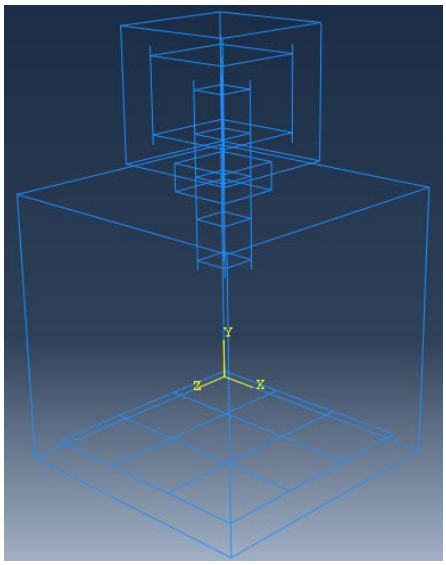

Figure 2. Concrete meshing.

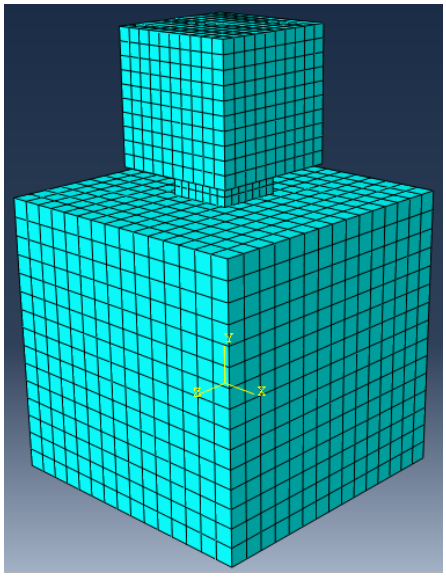

Figure 3. Steel reinforcement meshing.

2.3. Concrete damage plasticity

Concrete damaged plasticity method (CDP) was used to model the concrete behavior. The method was introduced on 1989 by Lubliner, and developed later on 1998 by Lee and Fenves [20–22]. Different parameters are used in the CDP to describe the nonlinear behavior of concrete, such as the cracking and inelastic strains, as well as stiffness degradation and other parameters. CDP method comprises majorly two independent behaviors in tension and compression as defined by stress strain graphs separately, Fig. 4. The concrete inelastic strain in compression "ε^{in}", and the cracking strain in tension "ε^{ck}" are:

$$\varepsilon^{in} = \varepsilon_c - \frac{\sigma_c}{E_0} \tag{1}$$

$$\varepsilon^{ck} = \varepsilon_t - \frac{\sigma_t}{E_0} \tag{2}$$

Where "σ_c" and "σ_t" are respectively the compressive and tensile stresses in concrete, and "E_0" is the initial modulus of elasticity.

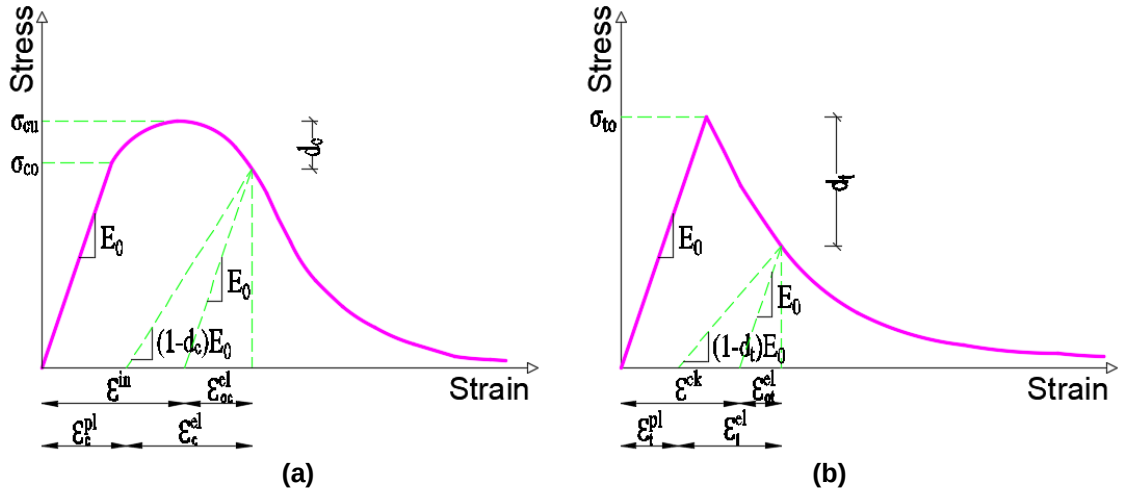

Figure 4. Uniaxial behavior of concrete: (a) under compression, (b) under tension.

Further, two isotropic damage parameters "d_c" and "d_t" are used accordingly to describe the stiffness degradation of concrete in compression and in tension respectively. The parameters are assigned as the concrete is strained beyond its elastic limit. The damage parameters have a maximum value of 1, where the material have reached full damage [23–26]. Equations 3 and 4 represents the damage parameters for compression and tension respectively.

$$d_c = 1 - \frac{\sigma_c}{E_0\left(\varepsilon_c - \varepsilon_c^{pl}\right)} \tag{3}$$

$$d_t = 1 - \frac{\sigma_t}{E_0\left(\varepsilon_t - \varepsilon_t^{pl}\right)} \tag{4}$$

Using the damage parameters, the inelastic and crack strains are then transferred into plastic strains at compression " ε_c^{pl} "and tension " ε_t^{pl} " as follows:

$$\varepsilon_c^{pl} = \varepsilon^{in} - \left(\frac{d_c}{1-d_c}\right)\left(\frac{\sigma_c}{E_0}\right) \tag{5}$$

$$\varepsilon_t^{pl} = \varepsilon^{ck} - \left(\frac{d_t}{1-d_t}\right)\left(\frac{\sigma_t}{E_0}\right) \tag{6}$$

The parameters provided were accomplished by following up a reliable approach in the triad "composition, structure, and properties" [27–29]. The concrete mechanical properties used in CDP are summarized in Table 2. The steel reinforcement was modeled using the elastoplastic behavior, and the mechanical properties of steel rebars are stated in Table 3.

Table 2. Mechanical properties of concrete.

Parameter	Unit	Symbol	Value		
Compressive strength	MPa	f'_c	22	32	40
Tensile strength	MPa	f_t	2.91	3.51	3.92
Elastic modulus	MPa	E_c	22,045	26,587	29,725
Poisson's ratio		ν	0.2		
Density	KN/m^3	ρ	2400		
Dilation angle	°	ψ	30		
Eccentricity		ε	0.1		
Bi-axial to uni-axial strength ratio		f_{b0}/f_{t0}	1.16		
Second stress invariant ratio		K	0.667		
Viscosity parameter		μ	0.00001		

Table 3. Mechanical properties of steel reinforcement.

Parameter	Unit	Symbol	Value
Yield strength	MPa	f_y	520
Ultimate strength	MPa	f_u	624
Elastic modulus	MPa	E_s	200,000
Poisson's ratio		ν	0.3
Density	KN/m^3	ρ	78.5

3. Results and Discussion

3.1. Model calibration

As mentioned earlier, the eighteen models were analyzed using ABAQUS software. An imposed displacement of 20 mm was applied only on the top center of the column's specimen of each model. As indicated earlier, ACI 318-14 limits the increase in strength due to confinement up to $\sqrt{A_c / A_h}$ = 2 [30]. The column sizes were increased as much as 16 times the hinge area in order to reach double the code limitation.

Several failure modes were experienced in the hinge area. Two-way hinges with low area ratios $\sqrt{A_c / A_h}$ = 2, mainly failed by hinge crushing as for models CS14-22, CS14-32 and CS14-40. The red volumes seen in Fig. 5 indicates the crushed concrete elements. The crushing starts from a distance up through the column. The stress concentrated in the failed zone and are transferred through the hinge. Fig. 6 describes the axial stress distribution throughout the model. The hinge axial capacity is amplified due to the confinement effect produced by the column on the throat area, even though it was not enough to withstand the vertical stress induced.

ABAQUS references the x, y and z axis as 1, 2 and 3 respectively. In the pure stresses states, tensile forces and stresses are positive while compressive forces and stresses are negative.

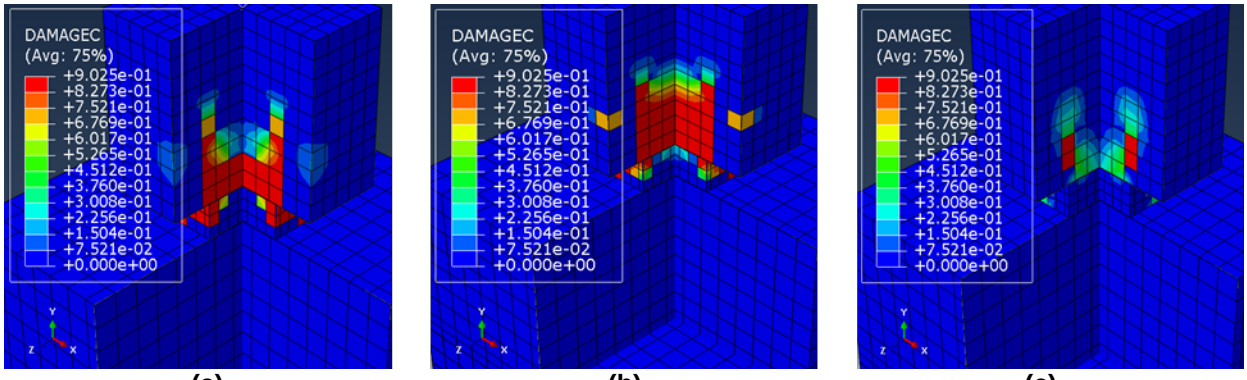

(a) **(b)** **(c)**

Figure 5. Hinge failure of two-way hinges with low area ratios: (a) SC14-22, (b) SC14-32, (c) SC14-40.

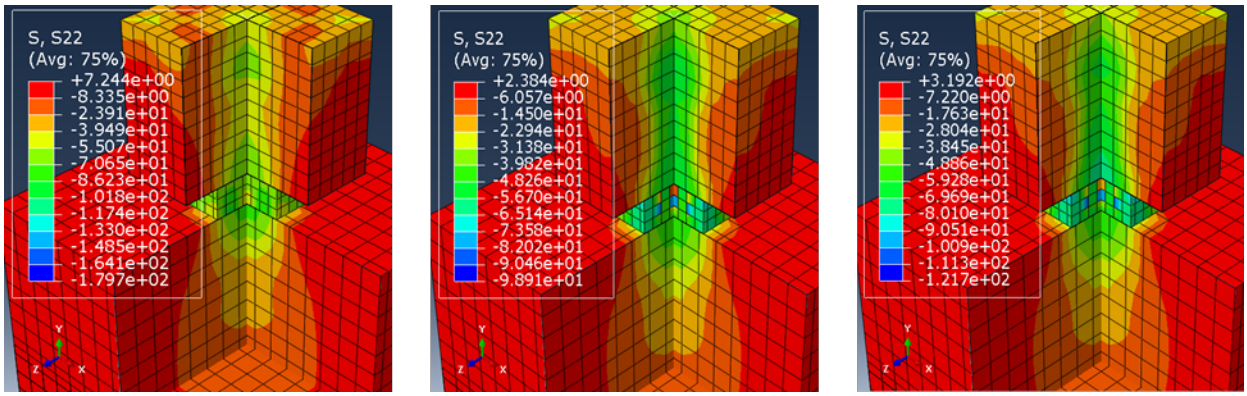

(a) **(b)** **(c)**

Figure 6. Vertical stress of two-way hinges with low area ratios: (a) SC14-22, (b) SC14-32, (c) SC14-40.

On the other hand, the next fifteen models with high area ratios $\sqrt{A_c / A_h} > 2$, failed by splitting failure above throat area. The red plan seen in Fig. 7 presents the shear failure plane, and the splitting failure above the hinge area is provided as well. Fig. 8 clarifies the spreading of stress S22 throughout the hinge. It was observed that the confining stress produced by the column on the throat area increased the hinge axial capacity to become greater than what the column can withstand.

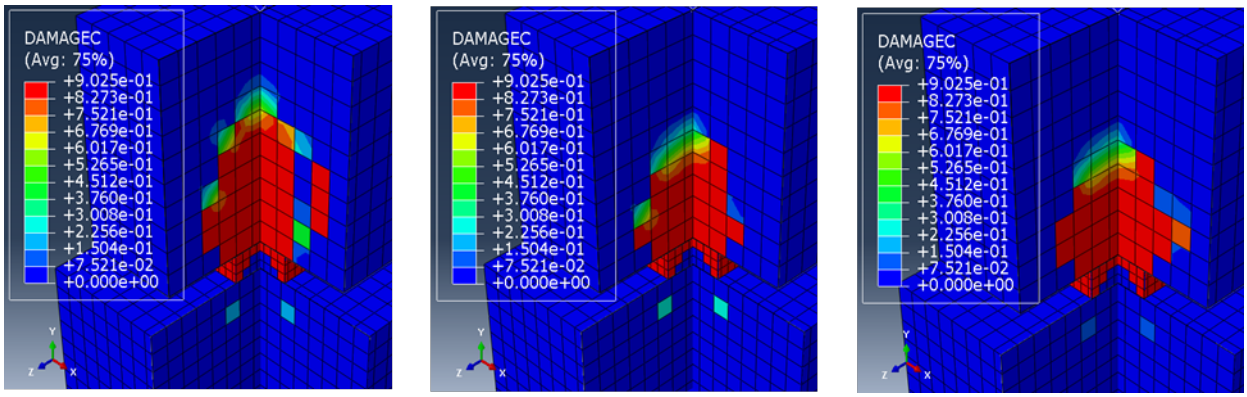

(a) **(b)** **(c)**

Figure 7. Splitting failure of two-way hinges with high area ratios: (a) SC23-22, (b) SC23-32, (c) SC23-40.

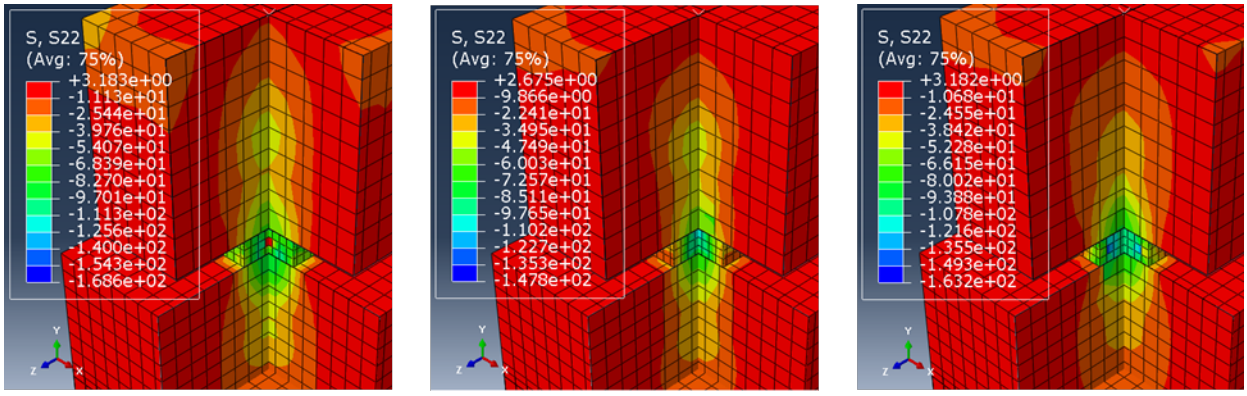

(a) **(b)** **(c)**

Figure 8. Vertical stress S22 of two-way hinges with high area ratios: (a) SC23-22, (b) SC23-32, (c) SC23-40.

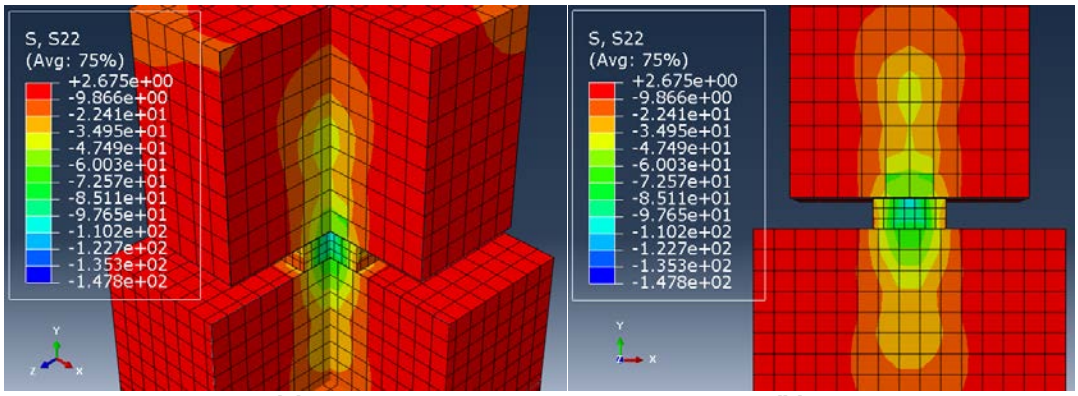

(a) **(b)**

Figure 9. CS23-32 vertical stress S22: (a) 3-D section, (b) Planner section.

The model CS23-32, $\sqrt{Ac / Ah}$ = 3.29, was selected to illustrate the transfer of stress through the hinge. ABAQUS references the x, y and z axis as 1, 2 and 3 respectively. In the pure stress states, the tensile stress is positive however the compressive stress is negative. Fig. 9 describes the vertical stress S22 distribution through the model CS23-32. The hinge reached the ultimate axial strength at a value of 115 MPa, which is way larger than the concrete compressive strength (32 MPa). The hinge axial capacity is amplified up due to the confining stresses S11 and S33 imposed by the larger area surrounding the throat region. The vertical Stress S22 in the column upper portion, where there is less confining effects is about 32 MPa. This demonstrates the abrupt increase in the stress as it passes through the smaller throat area. The stress concentrated at a distance approximately equal to half the width of the column.

Fig. 10 shows the lateral confining stresses S11 and S33 of CS23-32. It is obvious that the stresses are mainly provided at the hinge area. The maximum confining stress developed is in the range of 34 MPa, which highly amplifies the hinge bearing capacity.

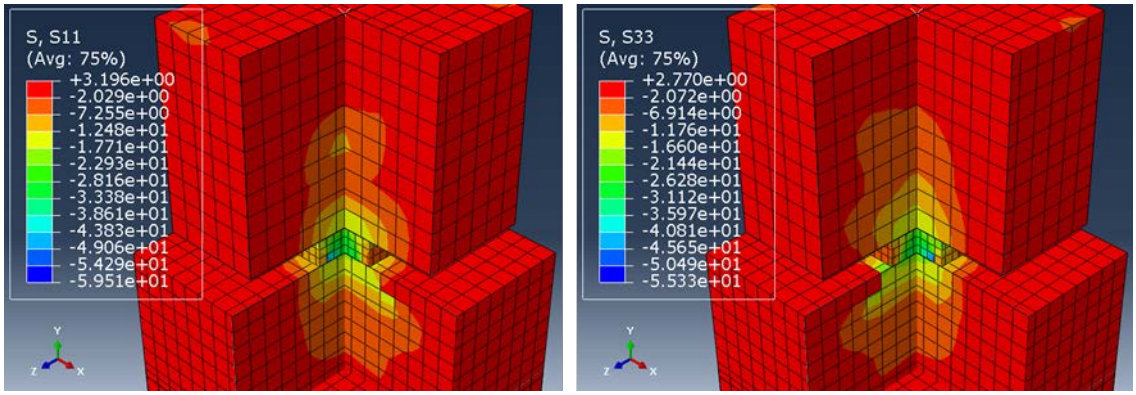

(a) **(b)**

Figure 10. CS23-32 lateral stresses: (a) stress S11, (b) stress S33.

On the other hand, consider the model CS14-32 which is a two-way hinge with a small area ratio, $\sqrt{Ac / Ah}$ = 2. Fig. 11 shows the distribution of vertical stress S22 through the hinge. The model reached the ultimate axial strength at a value of 85 MPa.

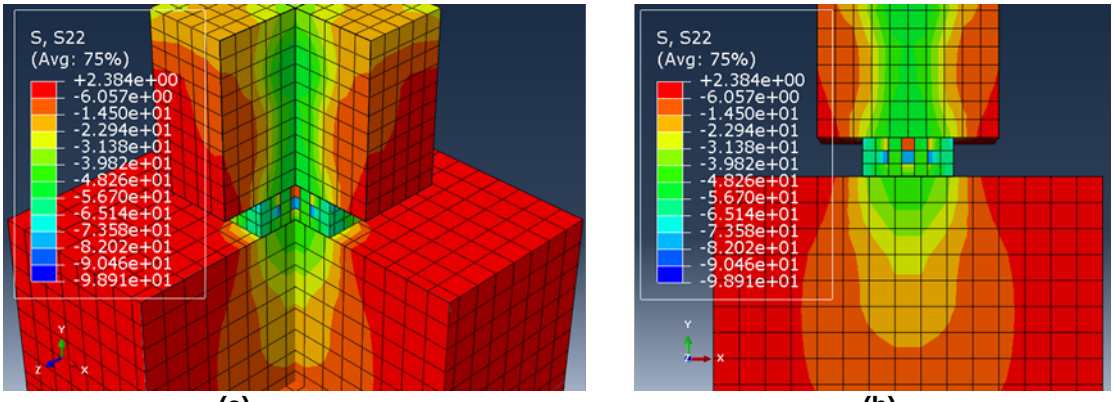

(a) **(b)**

Figure 11. CS14-32 vertical stress S22: (a) 3-D section, (b) Planner section.

The lateral confining stresses S11 and S33 of model CS14-32 are illustrated in Fig. 12. The model do not have enough distance to reach the optimum confining levels. The stresses S11 and S33 in the throat zone are both about to 14 MPa, which is much smaller than the corresponding lateral stress of CS23-32 (34 MPa).

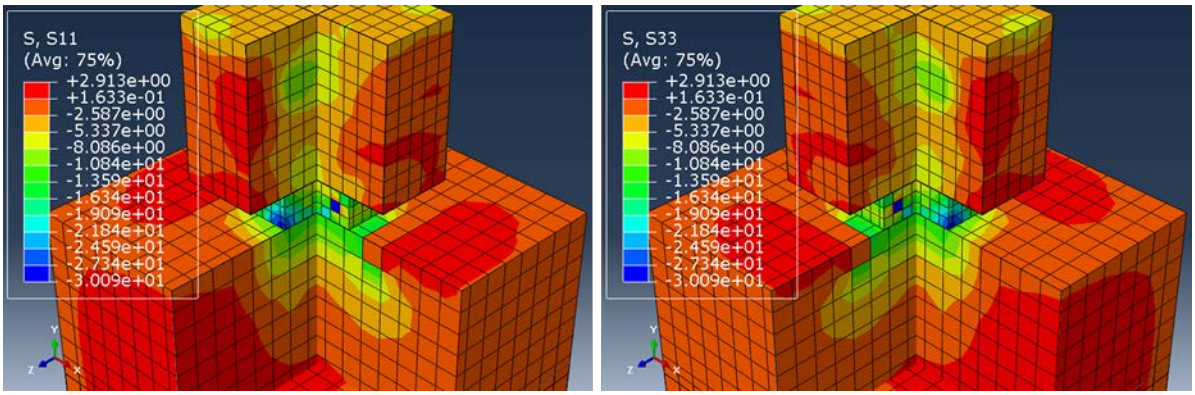

(a) **(b)**

Figure 12. CS14-32 lateral stresses: (a) stress S11, (b) stress S33.

Fig. 13 shows a comparison between the finite element analysis and experimental results of load displacement curves for CS14 and CS23 with the different concrete compressive strengths.

The load displacement curves due to the FEA for all cases are plotted in Fig. 14. The ABAQUS outcomes are in a very good agreement compared with the experimental results. Although all the models failed way before 20 mm displacement, the hinges with high area ratios exhibited ductile failure modes.

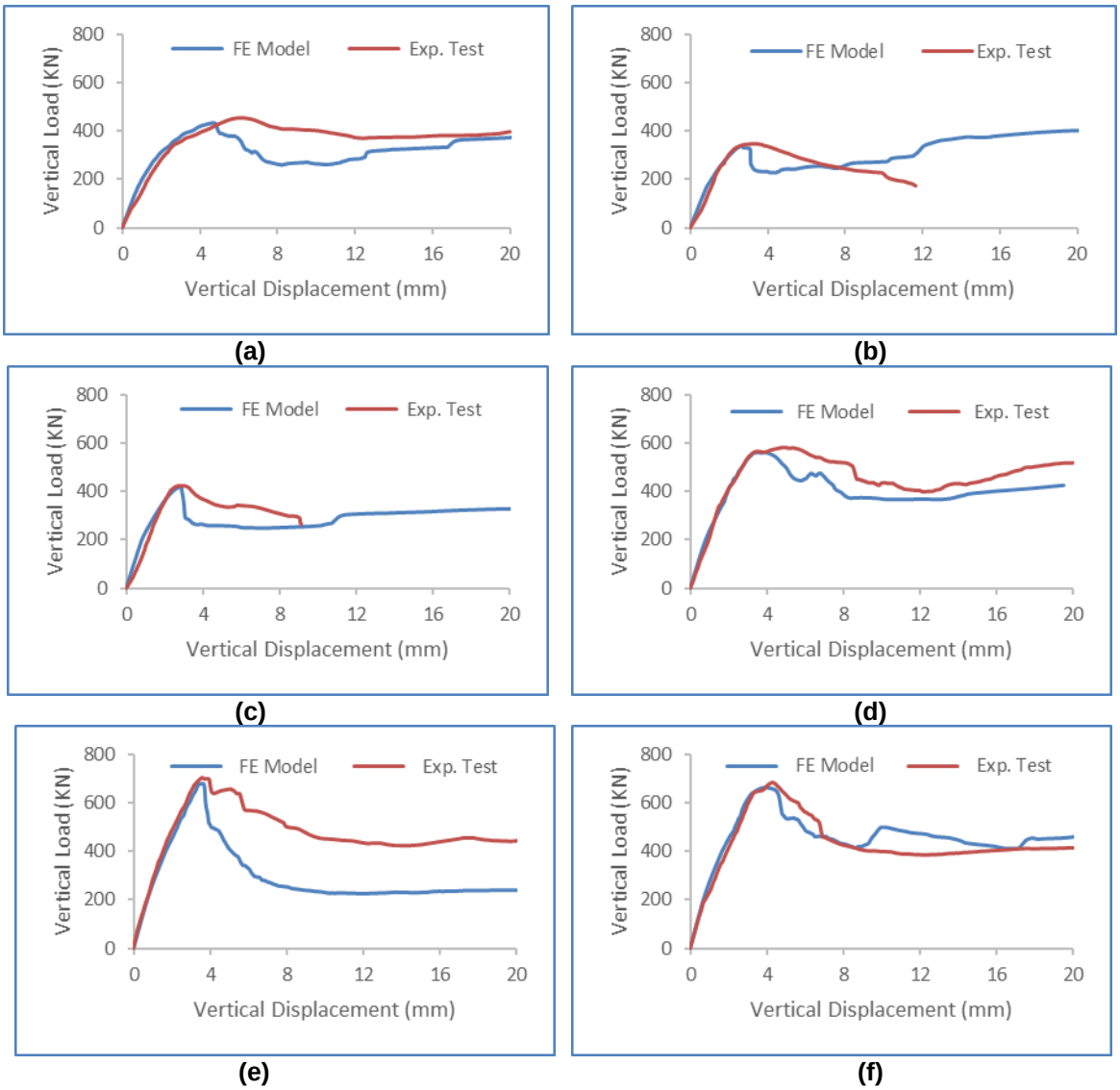

(a) **(b)**

(c) **(d)**

(e) **(f)**

Figure 13. FE model and experimental test of load displacement curves for CS14 and CS23: (a) CS14-22, (b) CS23-22, (c) CS14-32, (d) CS23-32, (e) CS14-40, (f) CS23-40.

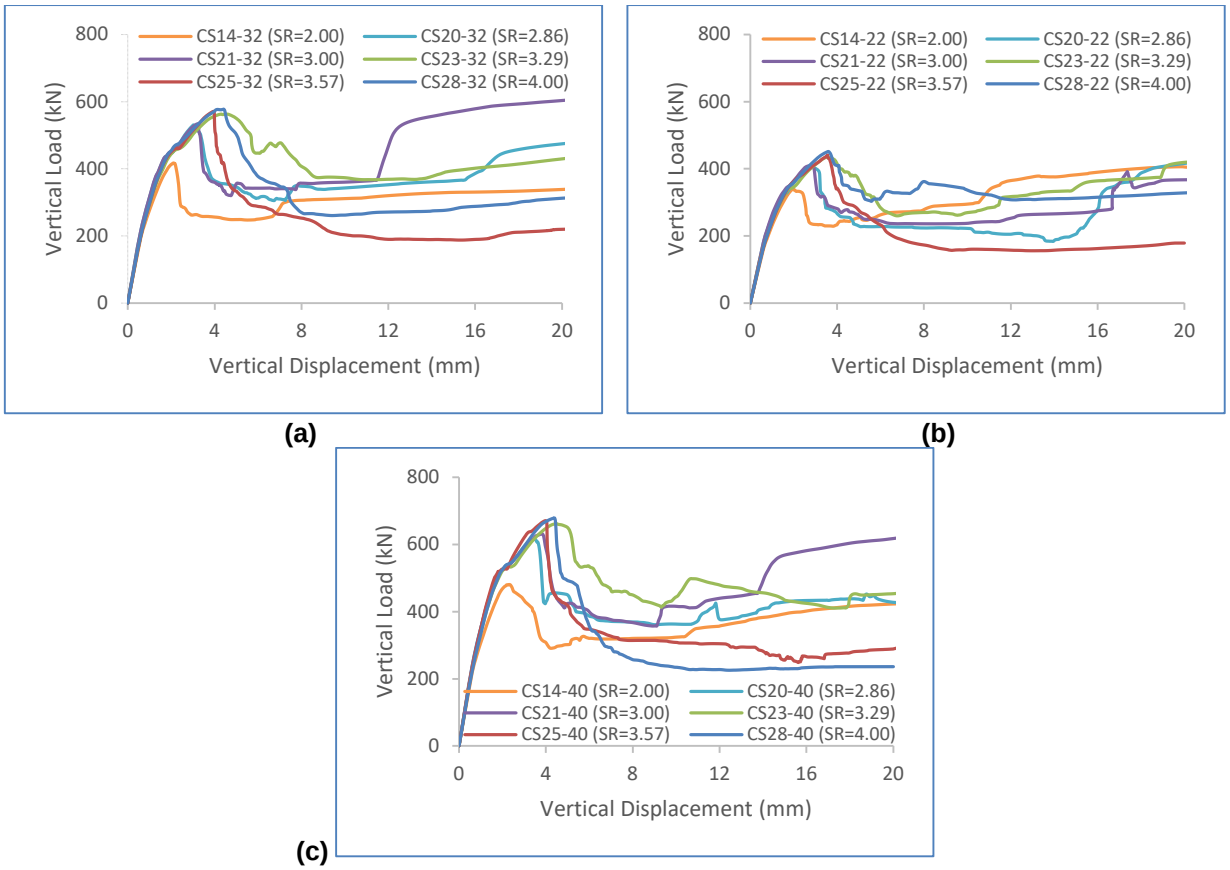

Figure 14. Axial load-displacement curves: (a) CS-22, (b) CS-32, (c) CS-40.

Fig. 15 displays the hinge axial capacity versus the square ratio of column to hinge area $\sqrt{Ac / Ah}$.

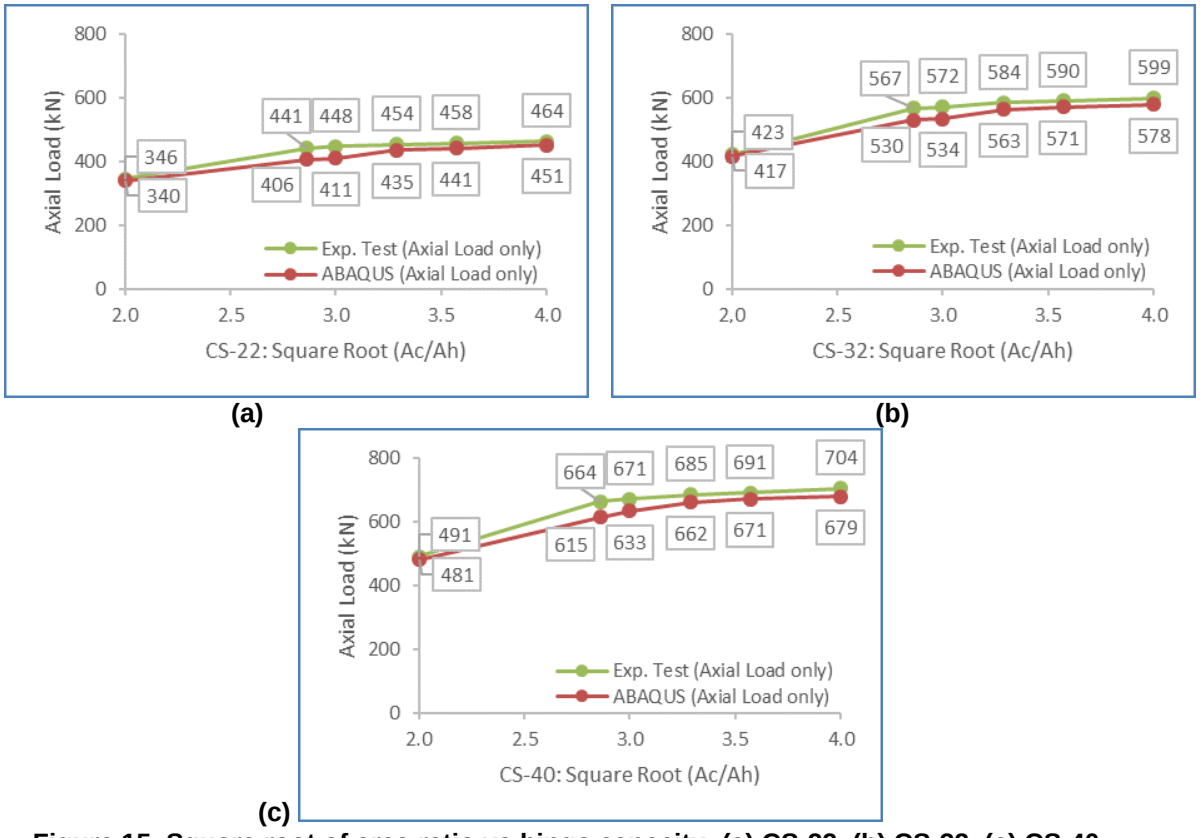

Figure 15. Square root of area ratio vs hinge capacity: (a) CS-22, (b) CS-32, (c) CS-40.

According to ACI Code, the hinge ultimate capacity P_{ulh} is:

$$P_{ulh} = 0.85 f'c(Ah - Ast)\sqrt{Ac / Ah} + fyAst \quad (7)$$

where A_h is the gross sectional area of the concrete hinge and A_{st} is the area of hinge reinforcement.

ACI code stipulates that the amplification factor "$\sqrt{A_c / A_h}$" is limited to two. Beyond that, the confinement effect produced by the larger area on the throat would not effectively amplify the hinge capacity even if the column area is increased. Following the ABAQUS results, two-way hinge capacity did not have the same limit as the code stipulates. Obviously, the hinge capacity was amplified up by a confinement factor "CF" equal to three (Eq. 8). Indeed, the confinement factors reached an asymptotic value equal to 3.5 as indicated in Table 4. Despite the code recommends using the amplification factor in case the hinge is confined from both directions, many design methods consider using the factor for one-way hinge as well.

$$CF = \frac{P_{ulh} - f_y A_{st}}{0.85 f'c(A_h - A_{st})} \quad (8)$$

Table 4. Hinge confinement factor (CF).

Model	$\sqrt{A_c / A_h}$	Hinge Axial Load (KN)		Confinement Factor "CF"
		Exp.	ABAQUS	
CS14-22	2.00	346	340	2.06
CS20-22	2.86	441	406	2.83
CS21-22	3.00	448	411	2.89
CS23-22	3.29	454	435	3.17
CS25-22	3.57	458	441	3.24
CS28-22	4.00	464	451	3.36
CS14-32	2.00	423	417	2.03
CS20-32	2.86	567	530	2.94
CS21-32	3.00	572	534	2.97
CS23-32	3.29	584	563	3.20
CS25-32	3.57	590	571	3.27
CS28-32	4.00	599	578	3.32
CS14-32	2.00	491	481	2.10
CS20-32	2.86	664	615	3.21
CS21-32	3.00	671	633	3.26
CS23-32	3.29	685	662	3.35
CS25-32	3.57	691	671	3.38
CS28-32	4.00	704	679	3.47

3.2. Model analysis due to the dual effect of axial and lateral loads

The finite element calibrated and verified the experimental work. The models were further analyzed, using ABAQUS, to investigate their behaviors under the dual effect of axial and lateral loads. Simultaneously, an imposed vertical displacement of 10 mm was applied at the top center of the column of each model, and a lateral displacement of 10 mm imposed at the center of the hinge thickness as well.

Several failure modes were observed. The models CS14-22, CS14-32 and CS14-40, with low area ratios $\sqrt{A_c / A_h}$ = 2, exhibited bearing failure at the throat region. As shown in Fig. 16, the red volumes presents the crushed concrete elements. The crushing starts from a distance up through the column. The deformation increased and the stiffness degraded through the test. The hinge reached the ultimate axial capacity before the shear slippage takes place. This implies that the confining stress produced by the column on the hinge was not enough to withstand the vertical stress induced. Fig. 17 describes the axial stress distribution of the cases mentioned. The stress concentrated but did not amplify the throat capacity. This is probably due to the presence of the shear stress which contributes in decreasing the hinge axial capacity by about 30~35 % as indicated next.

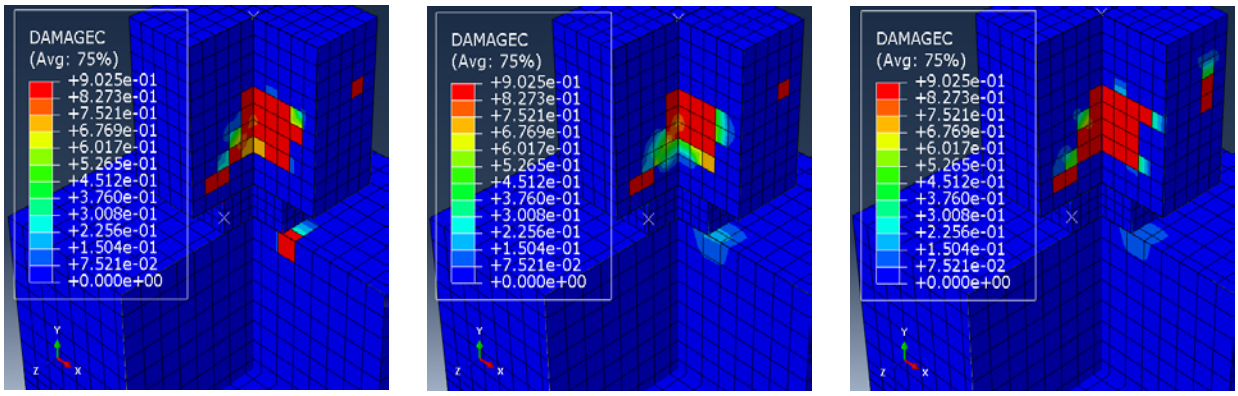

(a) **(b)** **(c)**

Figure 16. Hinge failure of two-way hinges with low area ratios: (a) SC14-22, (b) SC14-32, (c) SC14-40.

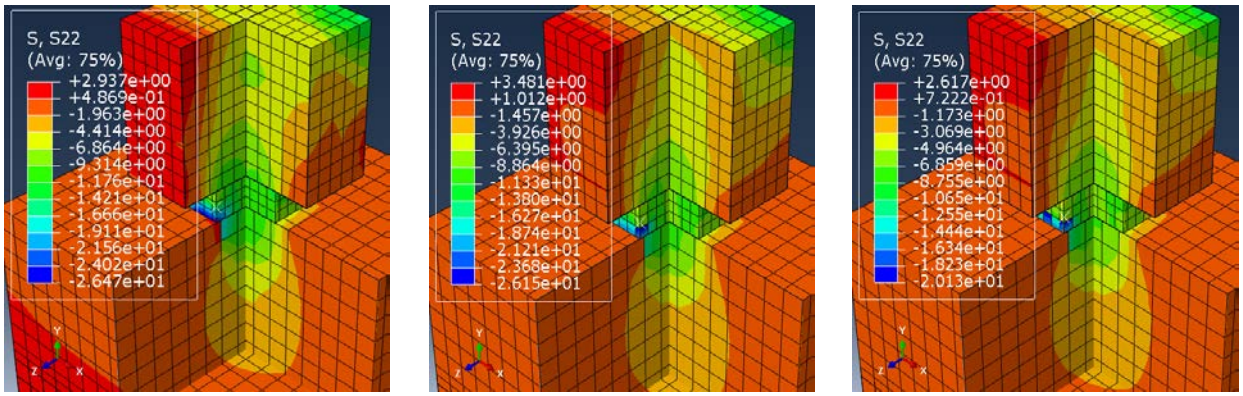

(a) **(b)** **(c)**

Figure 17. Vertical stress of two-way hinges with low area ratios: (a) SC14-22, (b) SC14-32, (c) SC14-40.

The models with high area ratios $\sqrt{Ac / Ah}$ > 2, failed by hinge-footing slippage interface as seen in Fig. 18. This indicates that the shear stress is greater than the confining stress produced by the column on the throat area. The red volume presents the concrete damage imposed by the shear slippage failure. It was observed that the deterioration was quite substantial right after the model reached the peak shear strength. Fig. 19 shows the stress distribution throughout the hinge. The stress concentrated and slightly amplified the throat axial capacity. Similarly to the above mentioned, the presence of the shear stress dropped the hinge axial capacity by about 30~35 %.

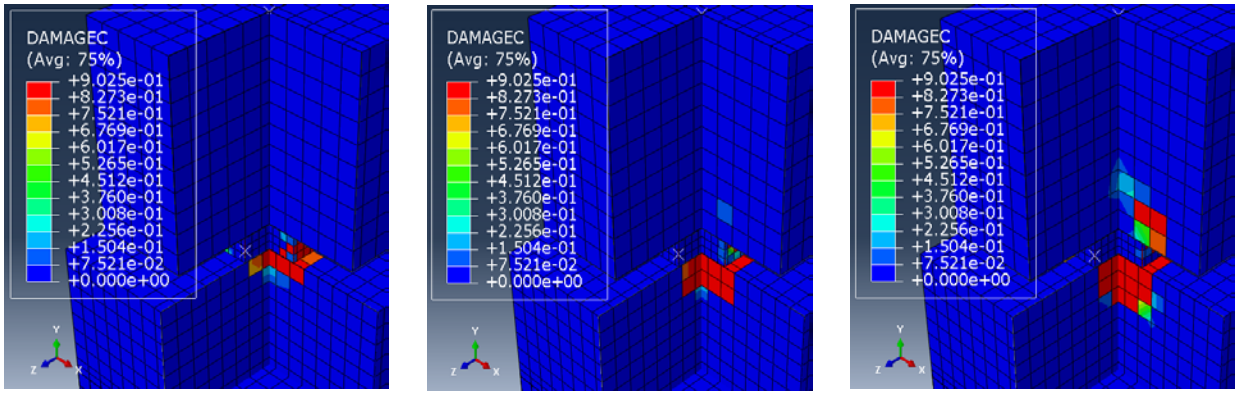

(a) **(b)** **(c)**

Figure 18. Shear slippage failure of two-way hinges with high area ratios: (a) SC23-22, (b) SC23-32, (c) SC23-40.

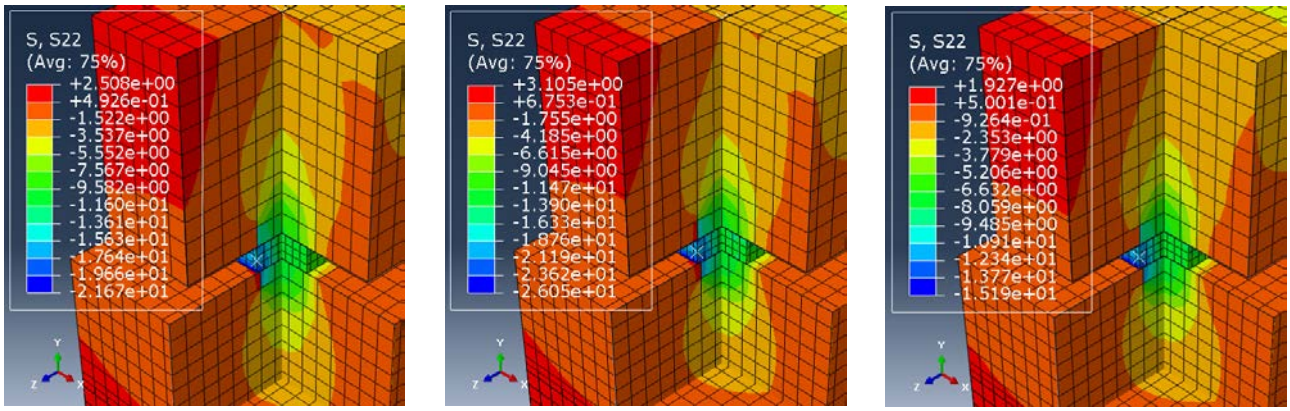

(a) **(b)** **(c)**

Figure 19. Vertical stress of two-way hinges with high area ratios: (a) SC23-22, (b) SC23-32, (c) SC23-40.

The drop of the hinge axial capacity is primarily due to the presence of the lateral shear stress which contributes in degrading the throat stiffness. As summarized in Table 5, the confinement factor "CF" is decreased to 1 for the hinges with low area ratios and to 1.5 for those with the high ones. Therefore, "CF" is not practically valuable. Fig. 20 presents the axial load displacement curves performed by ABAQUS for the different cases considered. Fig. 21 displays the hinge axial capacity versus the square root ratio of column to hinge area $\sqrt{Ac / Ah}$.

Table 5. Hinge axial capacity.

Model	$\sqrt{Ac / Ah}$	ABAQUS		Capacity Drop %	Confinement Factor (CF)
		(Axial Load only) KN	(Axial & Lateral Loads) KN		
CS14-22	2.00	340	235	31%	0.84
CS20-22	2.86	406	281	31%	1.37
CS21-22	3.00	411	284	31%	1.41
CS23-22	3.29	435	287	34%	1.44
CS25-22	3.57	441	291	34%	1.49
CS28-22	4.00	451	302	33%	1.62
CS14-32	2.00	417	278	33%	0.92
CS20-32	2.86	530	341	36%	1.42
CS21-32	3.00	534	346	35%	1.46
CS23-32	3.29	563	363	36%	1.60
CS25-32	3.57	571	370	35%	1.66
CS28-32	4.00	578	376	35%	1.71
CS14-40	2.00	481	314	35%	0.97
CS20-40	2.86	615	413	33%	1.60
CS21-40	3.00	633	420	34%	1.65
CS23-40	3.29	662	425	36%	1.68
CS25-40	3.57	671	431	36%	1.72
CS28-40	4.00	679	438	35%	1.76

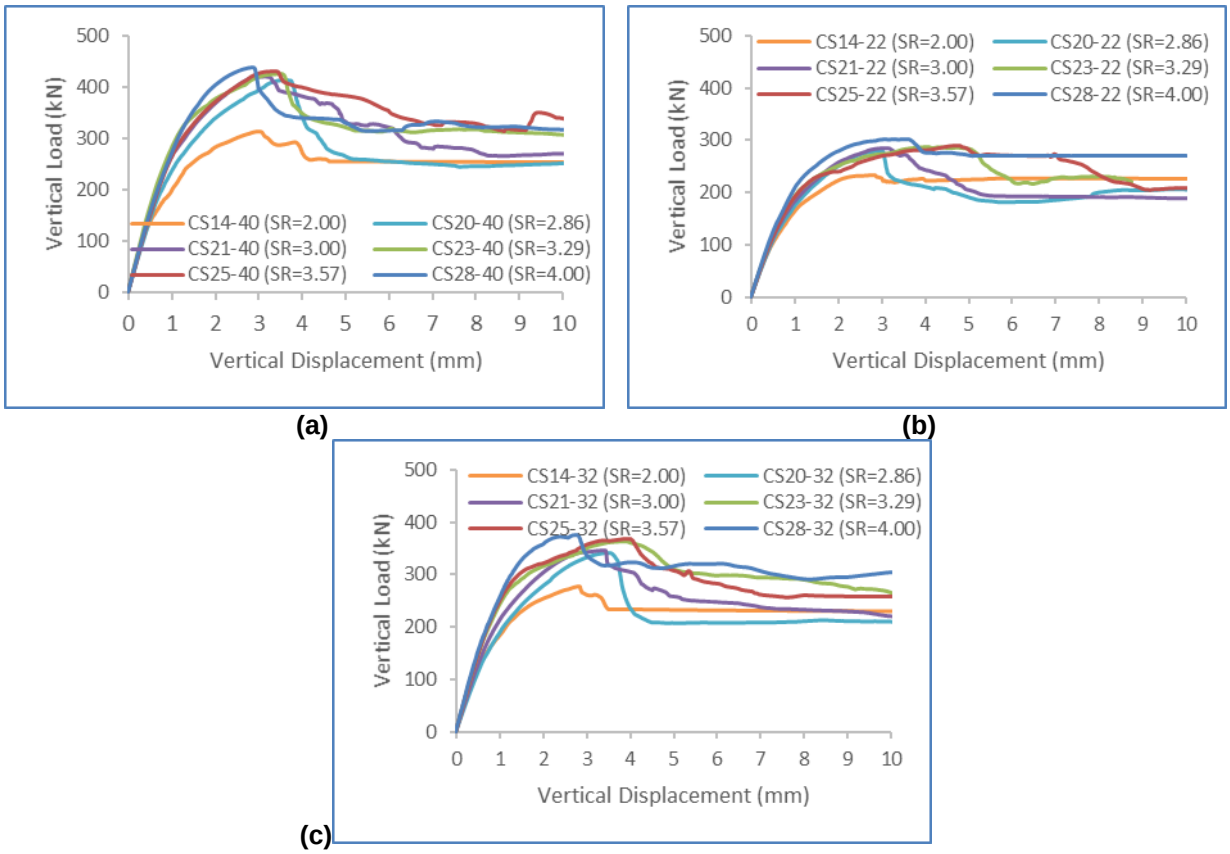

Figure 20. Axial load-displacement curves: (a) CS-22, (b) CS-32, (c) CS-40.

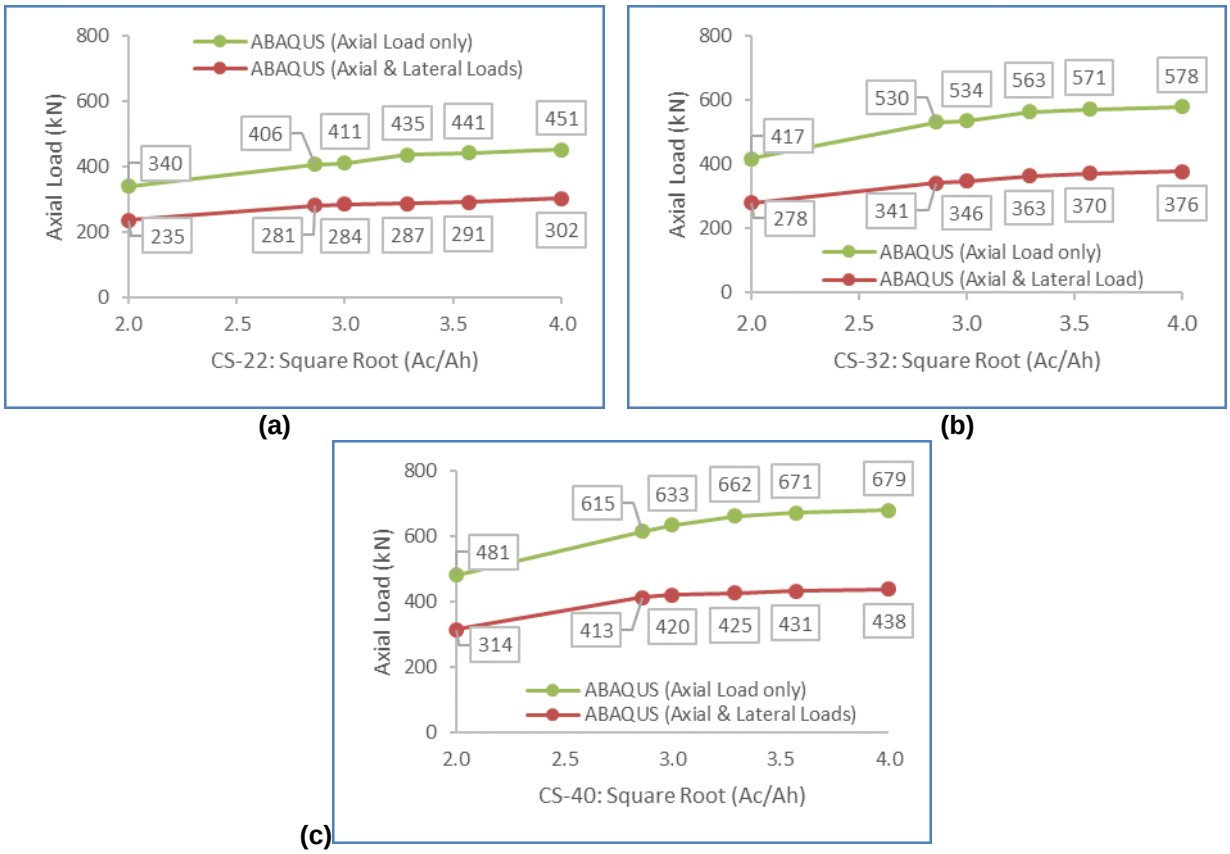

Figure 21. Square root of area ratio vs hinge capacity: (a) CS-22, (b) CS-32, (c) CS-40.

According to ACI code, the hinge nominal shear V_{hn} is [30–32]:

$$V_{hn} = \min\{0.2 f_c' A_c; (3.3 + 0.08 f_c') A_c; 11 A_c\} \quad (9)$$

The confining stress produced by the column on the throat area, has a great influence on the hinge shear strength. Regardless of the level of the column/hinge area ratio, the shear capacity of two-way hinges was five times higher than the code states, as indicated on Table 6. Fig. 22 presents the lateral load displacement curves performed by ABAQUS for the different cases considered.

Table 6. Hinge shear strength.

Model	$\sqrt{A_c / A_h}$	Hinge Shear Strength (KN)		Increasing Rate
		ACI Code	ABAQUS	
CS14-22	2.00	22	105	4.77
CS20-22	2.86	22	117	5.32
CS21-22	3.00	22	114	5.18
CS23-22	3.29	22	116	5.27
CS25-22	3.57	22	117	5.32
CS28-22	4.00	22	117	5.32
CS14-32	2.00	29	126	4.34
CS20-32	2.86	29	137	4.72
CS21-32	3.00	29	139	4.79
CS23-32	3.29	29	138	4.76
CS25-32	3.57	29	139	4.79
CS28-32	4.00	29	140	4.83
CS14-40	2.00	32	143	4.47
CS20-40	2.86	32	163	5.09
CS21-40	3.00	32	161	5.03
CS23-40	3.29	32	162	5.06
CS25-40	3.57	32	162	5.06
CS28-40	4.00	32	163	5.09

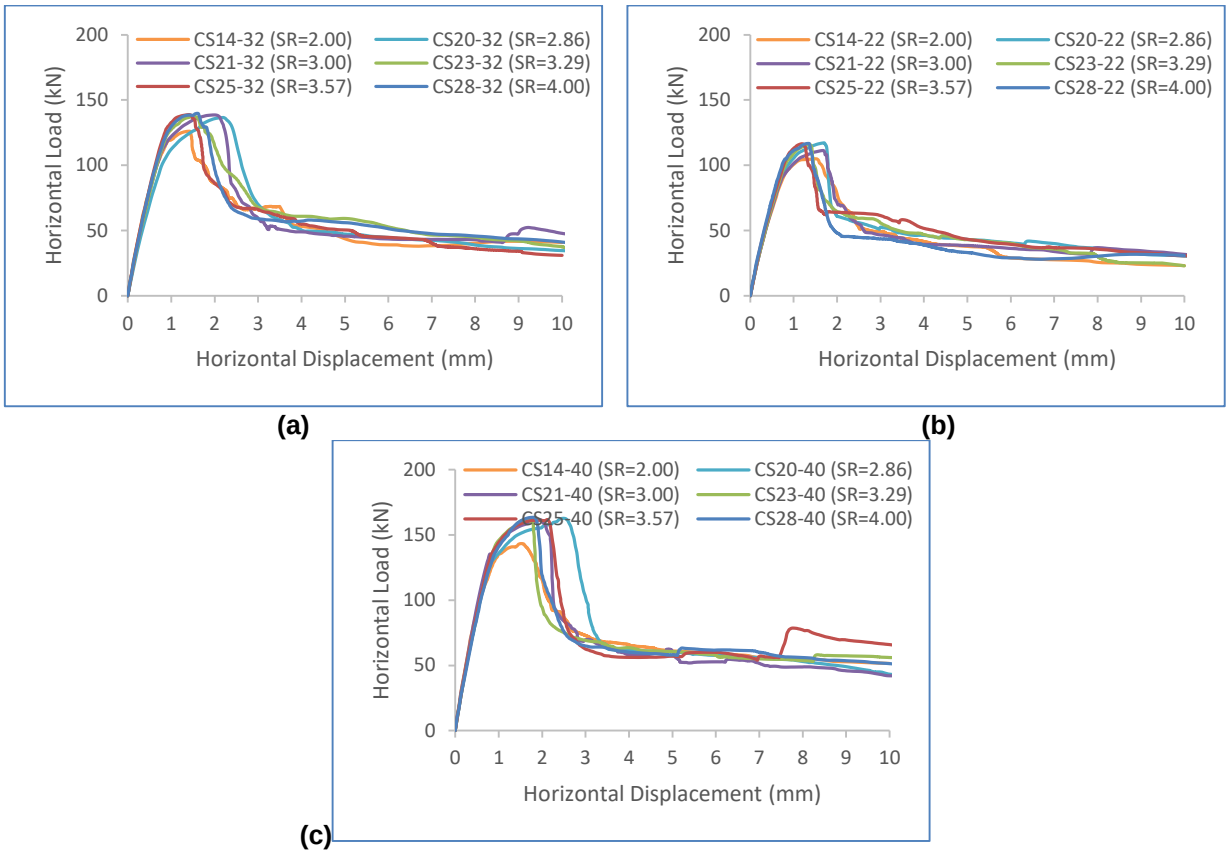

Figure 22. Lateral load-displacement curves: (a) CS-22, (b) CS-32, (c) CS-40.

4. Conclusions

This paper investigates the behavior of two-way hinges in reinforced concrete structures using the finite element method. The main conclusions are as follows:

1. The hinges with low area ratios $\sqrt{A_c / A_h}$ = 2, mainly failed by hinge crushing. This implies that the confining stress produced by the column on the hinge was not enough to bear the vertical stress induced. On the other side, the hinges with high area ratios $\sqrt{A_c / A_h}$ > 2, failed by splitting failure above throat area. This means that the confining stress produced by the column on the hinge was greater than what the column can withstand.

2. The hinges with high area ratios $\sqrt{A_c / A_h}$ > 2, exhibited ductile failure modes, noting that a large displacement was imposed by ABAQUS prior to complete failure. The transfer of stress through the hinge indicates that the hinges with high area ratios showed better confinement than those with low ratios.

3. Two-way hinge axial capacity did not have the same limit as the code stipulates. The capacity was noticeably amplified up by a confinement factor “CF” equal to three.

4. Subjected to the dual effect of lateral and axial loads, two-way hinges with low area ratios $\sqrt{A_c / A_h}$ = 2, exhibited bearing failure at the hinge region. This entails that the confining stress produced by the column on the hinge was not enough to withstand the vertical stress induced. However, the hinges with high area ratios $\sqrt{A_c / A_h}$ > 2, failed by hinge-footing slippage interface. This indicates that the confining stress increased the hinge bearing capacity and thereby, the hinge failed once the shear stress exceeded the shear capacity.

5. The confining stress produced by the column on the throat area has a great influence on the hinge shear strength. Regardless of the level of the column/hinge area ratio, the shear capacity of two-way hinges was five times higher than what the code states.

6. The presence of the shear stress decreased the axial capacity of the hinge by about 30~35 %, and the amplification factor due to the confinement effect was decreased to nearly 1 for the models with low area ratios and to 1.5 for those with the high ones.

References

1. Marx, S., Schacht, G. Concrete hinges in bridge engineering. Proceedings of the Institution of Civil Engineers, Engineering History and Heritage. 2015. 168(2). Pp. 64–74. DOI: 10.1680/ehah.14.00020
2. Griezic, A., Zeyl, P.E., Cook, W.D., Mitchell, D. Experimental studies of hinges in existing bridge columns. 7th Canadian Conference on Earthquake Engineering, Montreal. 1995.
3. Hillis, D., Saiidi, M.S. Construction and nonlinear dynamic analysis of three bridge bents used in a bridge system test. Center for Civil Engineering Earthquake Research, Department of Civil and Environmental Engineering, University of Nevada. 2009. Report No. CCEER-09-03. [Online]. https://scholarworks.unr.edu/handle/11714/7166. (Accessed: 05.04.2020).
4. Zaghi, A.E., Saiidi, M.S. Seismic performance of pipe-pin two-way hinges in concrete bridge columns. Journal of Earthquake Engineering. 2010. 14(8). Pp. 1253–1302. DOI: 10.1080/13632469.2010.490321
5. Zaghi, A.E., Saiidi, M.S. Bearing and shear failure of pipe-pin hinges subjected to earthquakes. ASCE Journal of Bridge Engineering. 2011. 16(3). Pp. 340–350. DOI: 10.1061/(ASCE)BE.1943-5592.0000160
6. Jiang, Y., Saiidi, M.S. Response and design of R/C one-way pier hinges in strong direction. ASCE Journal of Structural Engineering. 1995. 121(8). Pp. 1236–1244. DOI: 10.1061/(ASCE)0733-9445(1995)121:8(1236)
7. Saiidi, M.S., Cheng, Z.-Y, Sanders, D.L. An experimental study of two-way reinforced concrete column hinges under seismic load. ACI Structural Journal. 2009. 106(3). Pp. 340–348. DOI: 10.14359/56498
8. Saiidi, M.S., Orie, J., Douglas, B. Lateral load response of R/C bridge columns with a one-way pinned end. ACI Structural Journal. 1988. 85(6). Pp. 609–616. [Online]. https://www.researchgate.net/publication/296225889_Lateral_load_response_of_reinforced_concrete_bridge_columns_with_a_one-way_pinned_end. (Accessed: 05.04.2020).
9. McLean, D.I., Lim, K.Y. Moment-reducing hinge details for the bases of bridge columns. Washington State Department of Transportation. 1990. Report No. WA-RD 220.1. [Online]. https://www.wsdot.wa.gov/research/reports/fullreports/220.1.pdf. (Accessed: 05.04.2020).
10. Yuan, F., Wu, Y.F. Effect of load cycling on plastic hinge length in RC columns. Engineering Structures. 2017. 147. Pp. 90–102. DOI: 10.1016/j.engstruct.2017.05.046
11. Doyle, K.A., Saiidi, M.S. Seismic response of telescopic pipe pin connections. Center for Civil Engineering Earthquake Research, Department of Civil Engineering, University of Nevada. 2008. Report No. CCEER-08-01. [Online]. https://wolfweb.unr.edu/homepage/saiidi/caltrans/Pipe-Pins/PDFs/CCEER%2008_1.pdf. (Accessed: 05.04.2020).
12. Roberts, J.E. Caltrans structural control for bridges in high-seismic zones. Earthquake Engineering & Structural Dynamics. 2005. 34(4–5). Pp. 449–470. DOI: 10.1002/eqe.439
13. Mehrsoroush, A., Saiidi, M.S. Earthquake-resistant telescopic pipe pin column base connections for accelerated bridge construction. 10th U.S. National Conference on Earthquake Engineering, Frontiers of Earthquake Engineering. 2014. Alaska. DOI: 10.4231/D37S7HT0V
14. Mehrsoroush, A., Saiidi, M.S. Cyclic Response of Precast Bridge Piers with Novel Column-Base Pipe Pins and Pocket Cap Beam Connections. ASCE Journal of Bridge Engineering. 2016. 21(4): 04015080. DOI: 10.1061/(ASCE)BE.1943-5592.00-00833

15. Cheng, Z., Saiidi, M.S., Sanders, D. Development of a seismic design method for reinforced concrete two-way bridge column hinges. Center for Civil Engineering Earthquake Research, Department of Civil Engineering, University of Nevada. 2006. Report No. CCEER-06-01. [Online]. https://www.nevadadot.com/home/showdocument?id=3858. (Accessed: 05.04.2020).
16. Saiidi, M.S., Straw, D. Monotonic and cyclic response of one-way R/C Bridge pier hinges in the strong direction. ACI Structural Journal. 1993. 90(5). Pp. 568–573. [Online]. https://trid.trb.org/view/382330. (Accessed: 05.04.2020).
17. Chahal, S., Baalbaki, O., Timsah, Y., Ghanem, H., Abu Saleh, Z. Experimental Investigation of Two-Way Hinges in Reinforced Concrete Members. Proceedings of the 3rd GeoMEast International Congress and Exhibition. 2019. Pp. 128–146. DOI: 10.1007/978-3-030-34216-6_9
18. Chaudhari, S., Chakrabarti, M. Modeling of concrete for nonlinear analysis Using Finite Element Code ABAQUS. International Journal of Computer Applications. 2012. 44(7). Pp. 14–18. DOI: 10.5120/6274-8437
19. Wahalathantri, B.l., Thambiratnam, D.p., Chan, T.H.T., Fawzia, S. A material model for flexural crack simulation in reinforced concrete elements using Abaqus. Proceedings of the First International Conference on Engineering, Designing and Developing the Built Environment for Sustainable Wellbeing, Queensland University of Technology, Brisbane, Qld. 2011. Pp. 260–264. [Online]. https://eprints.qut.edu.au/41712/. (Accessed: 05.04.2020).
20. Kmiecik, P., Kaminski, M. Modelling of reinforced concrete structures and composite structures with concrete strength degradation taken into consideration. Archives of civil and mechanical engineering. 2011. 11(3). Pp. 623–636. DOI: 10.1016/S1644-9665(12)60105-8
21. Lubliner. J., Oliver. J., Oller. S., Onate. E. A plastic-damage model for concrete. International Journal of Solids and Structures. 1989. 25(3). Pp. 299–326. DOI: 10.1016/0020-7683(89)90050-4
22. Szczecina, M.S., Andrzej, W. Calibration of the CDP model parameters in Abaqus. The 2015 World Congress on Advances in Structural Engineering and Mechanics (ASEM15), Korea. 2015. [Online]. https://www.academia.edu/32626413/Calibration_of_the_CDP_model_parameters_in_Abaqus. (Accessed: 05.04.2020).
23. Lee, J., Fenves, G.L. Plastic-damage model for cyclic loading of concrete structures. Journal of Engineering Mechanics. 1998. 124(8). Pp. 892–900. DOI: 10.1061/(ASCE)0733-9399(1998)124:8(892)
24. Jankowiak, T., Lodygowski, T. Identification of parameters of concrete damage plasticity constitutive model. Foundations of Civil and Environmental Engineering, Poznan University of Technology. 2005. No. 6. Pp. 53–69. ISSN 1642–9303. [Online]. https://www.academia.edu/9635025/F_IDENTIFICATION_OF_PARAMETERS_OF_CONCRETE_DAMAGE_PLASTICITY_CONSTITUTIVE_MODEL. (Accessed: 05.04.2020).
25. Genikomsou, A.S., Polak, M.A. Finite element analysis of punching shear of concrete slabs using damage plasticity model in ABAQUS. Engineering Structures. 2015. 98. Pp. 38–48. DOI: 10.1016/j.engstruct.2015.04.016
26. Jahami, A., Temsah, Y., Khatib, J. The efficiency of using CFRP as a strengthening technique for reinforced concrete beams subjected to blast loading. International Journal of Advanced Structural Engineering. 2019. 11(4). Pp. 411–420. DOI: 10.1007/s40091-019-00242-w
27. Fediuk, R.S., Lesovik, V.S., Liseitsev, Y.L., Timokhin, R.A., Bituyev, A.V., Zaiakhanov, M.Y., Mochalov, A.V. Composite binders for concretes with improved shock resistance. Magazine of Civil Engineering. 2019. 85(1). Pp. 28–38. DOI: 10.18720/MCE.85.3
28. Fediuk, R.S., Lesovik, V.S., Mochalov, A.V., Otsokov, K.A., Lashina, I.V., Timokhin, R.A. Composite binders for concrete of protective structures. Magazine of Civil Engineering. 2018. 82(6). Pp. 208–218. DOI: 10.18720/MCE.82.19
29. Fediuk, R., Smoliakov, A., Muraviov, A. Mechanical properties of fiber-reinforced concrete using composite binders. Advances in Materials Science and Engineering. 2017. Article ID 2316347. Pp. 1–14. DOI: 10.1155/2017/2316347
30. Building code requirements for structural concrete (ACI 318-19). American Concrete Institute. 428 p, 433 p. DOI: 10.143-59/51716937
31. MacGregor, J., Wight, J. Reinforced Concrete Mechanics and Design. 6th edition. Pearson Education. New Jersey, 2012. 858 p.
32. Hassoun, M., Al-Manaseer, A. Structural Concrete Theory and Design. 6th edition. John Wiley & Sons. New Jersey, 2015. 456 p.

Contacts:

Safwan Chahal, safwanchahal79@gmail.com
Oussama Baalbaki, obaalbaki@bau.edu.lb
Yehia Temsah, ytemsah@bau.edu.lb
Hassan Ghanem, h.ghanem@bau.edu.lb
Zaher Abu Saleh, abousalehza@rhu.edu.lb